Flow visualization of liquid hydrogen line chilldown tests

Enrique Ramé*
National Center for Space Exploration Research
Jason W. Hartwig† and John B. McQuillen ‡
NASA Glenn Research Center, Cleveland, Ohio, 44135, USA

We present experimental measurements of wall and fluid temperature during chill-down tests of a warm cryogenic line with liquid hydrogen. Synchronized video and fluid temperature measurements are used to interpret stream temperature profiles versus time. When cold liquid hydrogen starts to flow into the warm line, a sequence of flow regimes, spanning from all-vapor at the outset to bubbly with continuum liquid at the end can be observed at a location far downstream of the cold inlet. In this paper we propose interpretations to the observed flow regimes and fluid temperature histories for two chilldown methods, viz. trickle (i.e. continuous) flow and pulse flow. Calculations of heat flux from the wall to the fluid versus wall temperature indicate the presence of the transition/nucleate boiling regimes only. The present tests, run at typical Reynolds numbers of $\sim O(10^5)$, are in sharp contrast to similar tests conducted at lower Reynolds numbers where a well-defined film boiling region is observed.

Nomenclature

θ	dimensionless fluid temperature
θ_w	dimensionless wall temperature
H	dimensionless heat transfer coefficient for fluid equation
H_w	dimensionless heat transfer coefficient for wall equation
Pe	Péclet number
Re	Reynolds number, $\dot{m}/\mu_L D$
T_o	Outer wall temperature (degrees Kelvin)
$\dot{m}$	Mass flow rate
D	Tube diameter
μ_L	Liquid viscosity
n_{on}	number of seconds a pulse flow is on
n_{off}	number of seconds a pulse flow is off

I. Introduction

Chilldown is defined as the process of cooling pipelines and components down to cryogenic temperatures so that single-phase liquid can eventually flow. Chilldown has been studied since the 1960s. The most relevant applications of chilldown are for in-space cryogenic engines and proposed cryogenic depots, defined as orbiting propellant stations in Low Earth Orbit where an empty spacecraft could rendezvous, dock, and refill before propellant resupply. Due to the overwhelming cost of launching and storing propellant in space, the chilldown process of depot transfer line and customer receiver tank must be optimized. Differences between the two chilldown schemes for depot transfer lines and for engine lines are depicted in Table 1. For example, engine chill down is generally optimized for short chilldown times while the proposed fuel depots will likely be optimized to conserve propellant mass.

Before in-space engine restart, chilldown of all the hardware between storage tank and engine is required. The Saturn V rocket used liquid hydrogen/liquid oxygen (LH2/LOX) RL-10 and J-2 engines for its upper stages[1]. Schuster *et al.*[2] studied the behavior of an RL10E-1 engine during chilldown using liquid hydrogen and liquid oxygen. Further details regarding the RL10E-1 and its reliability were discussed by Santiago[3], Van Lerberghe *et al.*[4], and Silke *et al.*[5].

For line chill down experiments, Yuan *et al.*[6] ran experiments to characterize laminar liquid nitrogen (LN2) flows for Reynolds number $(Re \equiv \dot{m}/\mu_L D) < 800$ within a horizontal tube under microgravity and in 1-g, and showed that heat transfer between fluid and wall is reduced in microgravity due to inverted annular flow. Kawanami *et al.*[7,8] investigated flow boiling of turbulent LN2 flows. Zhang & Fu[9] conducted LN2 chill down tests with vertical microtubes for

*c/o NASA Glenn Research Center, MS 110-3, Cleveland, Ohio, 44135, USA, Non-Member
†Propulsion and Propellants Branch, NASA Glenn Research Center, Cleveland, Ohio, 44135, USA, AIAA Member.
‡Senior Aerospace Engineer, Fluid Physics and Transport Branch, NASA Glenn Research Center, Cleveland, Ohio, 44135, USA, Non-Member.

Engine line	Transfer line
Large OD line	Small OD line
Short line ($<$ 1 m)	Long line (few meters)
Large flow demands	Small flow demands
Very short times (minutes)	Longer times ($\sim$ hour)
Propellant fed directly to engine	Multiple methods to chill
for line/engine chill down	down transfer line
Time-optimized	Mass-optimized

Table 1. Process-based differences between engine and transfer line chill.

$2300 < Re < 6700$. Hu *et al.*[10] conducted a comprehensive study into trickle flow and heat transfer in vertical pipes and also reported LN2 visualization while Shaeffer *et al.*[11] studied the effects of pulse and trickle LN2 flows within a vertical pipe. While trickle flows achieved faster chill down times, pulse flows consumed less mass.

While low Re number chilldown data and flow visualization exists for LN2 systems[6,10,12], there is only one known study conducted at high Re for liquid hydrogen by Brennan[13], but there was no flow visualization for that system. Scaling analyses and trade studies from Hartwig *et al.*[14] have shown that future cryogenic depots will likely operate at these higher flow rates, therefore necessitating the fundamental characterization of chill down at higher Re. Given that deep space missions will need to be resupplied with fuel, characterizing the dynamics of depot transfer line chilldown takes on renewed importance. This paper presents preliminary analyses and flow visualization for the recently conducted high Re number liquid hydrogen line chill down experiments at the NASA Glenn Research Center.

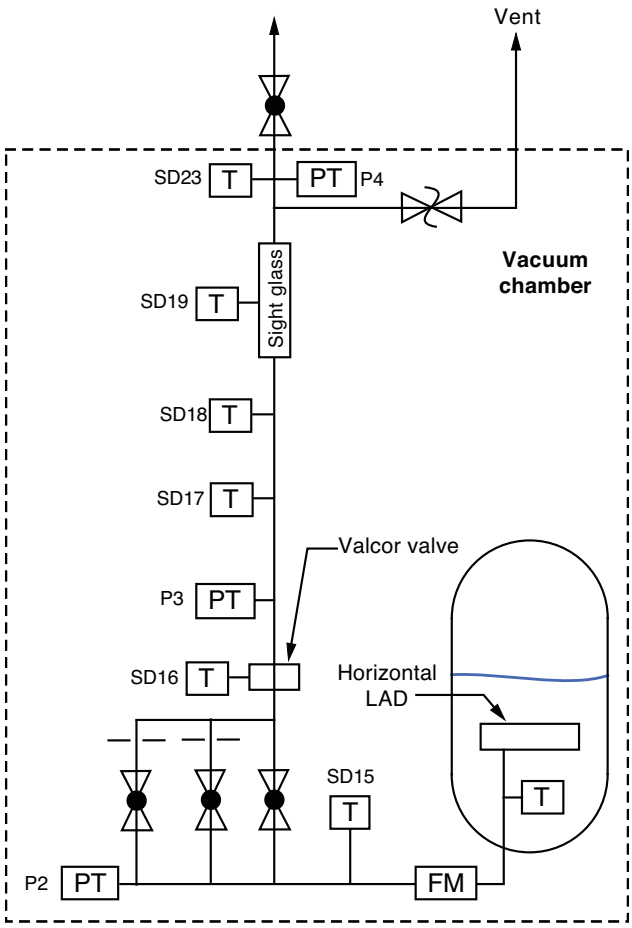

Figure 1. Schematic of the chill down lines showing the test section line. Three can be seen at the bottom, two of which have an orifice restriction to control low and medium flows; the third valve is a control valve, used in the high flow tests. The pressure transducers are marked as P[N] and silicon diode temperature transducers as SD[N], respectively, where [N] is a number. The flow meter is marked FM.

II. Hardware description

A. Fluid piping and instrumentation

The test section used in the chilldown tests was constructed with 0.5 inch OD stainless steel tubing and was 2.26 m (89 in) long. The flow could be observed near the downstream end of the line by means of a sight glass section inserted in the flow line at about 1.86 m (73.2 in) downstream of the line inlet. Fig. 1 shows a schematic of the system.

Liquid hydrogen was contained in a tank, and was fed to the lines through the outflow line of the horizontal LAD installed in the tank. The tank was pressurized with helium. Flow orifices were limiting restrictions that controlled low and medium flow, while a control valve was the limiting restriction that controlled high flow. The instrumentation for the test section can be seen in fig. 1, where SD are silicon diode temperature transducers, P are pressure transducers, and FM is the flow meter. The sight glass was used to observe the flow regime in the last portion of the line. The temperature and pressure taps (SD23 and P4) just downstream of the sight glass were installed in a T-fitting. Temperature probe SD23 sensed the stream temperature, while the other probes were skin diodes set up to measure wall temperatures.

Pressure and temperature conditions of the hydrogen in the tank were controlled by setting the tank pressure the evening before, and allowing the hydrogen to come to equilibrium. These conditions could not be maintained indefinitely, as the hydrogen temperature would rise over time due to injection of warmer helium as pressurant, but the temperature of the liquid was constant for the duration of every test.

B. Optics and video

A Dalsa camera was fitted with a board capable of 800 frames per second at a resolution of 1024 x 110 pixels. A compact C-mount lens from Schneider Optics covered a field of view of 6" by 0.5", adequate for the sight glass. A custom fiber optic backlit panel provided back illumination to the entire field of view.

The images clearly show the difference between liquid-covered and vapor-covered tube wall. When the wall is covered with liquid, the image of the edge of the tube shows a thin black shadow; when the wall is covered with vapor, the shadow on the tube edge image is significantly thicker, see fig. 2. The image shows all vapor on the right; on the left, a liquid layer can be seen at the wall, surrounding a vapor core. At the conditions of this frame, the remaining liquid hydrogen is rapidly evaporating. Shortly after this frame was taken, the entire field of view would be filled with vapor.

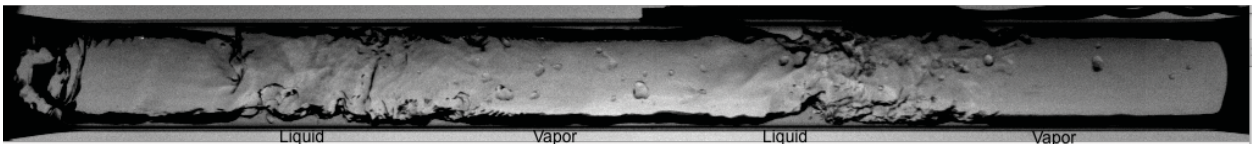

Figure 2. Video frame shortly after flow has stopped at the end of a test, showing the tube wall covered with vapor or liquid, as indicated with labels on the picture. Liquid hydrogen flowed from left to right.

III. Test types: general observations

Two types of flow strategy were used for the line chill-down, namely, trickle (fig. 3) and pulse (fig. 4). In both cases the flow rate of hydrogen flow could be set at low ($\dot{m} \approx 1$ lb/min), medium ($\dot{m} \approx 2$ lb/min) or high ($\dot{m} \approx 3$ lb/min). During a trickle flow set, the hydrogen was injected continuously into the chill-down test section. In the pulse test hydrogen flowed for n_{on} seconds, followed by n_{off} seconds of zero flow; hence the nomenclature 'n_{on}-n_{off}' pulse. All the data discussed in this paper are 'medium flow' (either trickle or pulse) tests.

Comparing the time histories of the two strategies, the pulsing character is clearly observable in figs. 4 and 5. Fig. 5 shows that, while the pulse maximum steady flow rate is about 1.6 lb/min (about 80% of the steady trickle flow rate), the cumulative mass spent in pulse flow is only 30% of that in trickle flow due to the off-time during pulsing. In both tests, the stream temperature SD23 drops to a constant minimum value (the 'bottom-out' time) after which the temperature is virtually equal to T_{sat} at the prevailing pressure. The pulse flow, flowing a lower averaged flow rate, takes longer but spends less mass than the normal trickle to achieve the bottom-out condition.

However, minimizing mass *and* time to bottom-out is important, so we compare –perhaps naïvely– the product of the total mass times the time to bottom out, $M_{\text{tot}} \times t_{\text{bot}}$. In this comparison, the pulse (17 lb.min) is more favorable than trickle (28.3 lb.min) in our configuration.

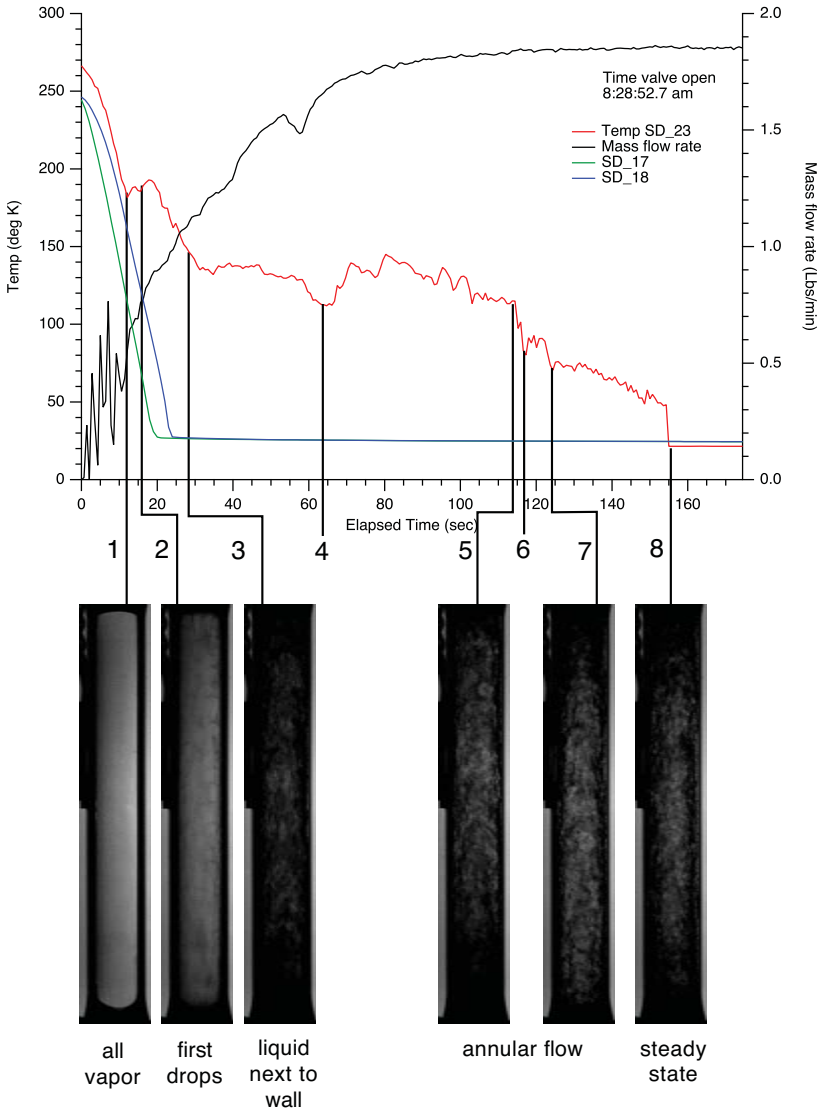

Figure 3. Time history of a medium trickle flow test. The photos below the plot illustrate the flow regime at the indicated time during the evolution of the stream temperature just after the sight glass (see fig. 1, temperature SD23). Flow direction is up.

IV. Basic physics and flow visualization

Fig. 3 shows time histories of two wall temperatures (SD17 and SD18), the stream temperature just downstream of the sight glass (SD23) and mass flow rate. The two skin diodes measuring wall temperature bottom out to steady temperature in succession, which would allow one to estimate a velocity for the quench front. These two temperature plots do not exhibit special features besides the sharp drop into the steady state temperature.

The stream temperature, on the other hand, shows a complex structure before bottoming out to the steady state. The sight glass was crucial in providing good information of flow characteristics, with video recordings at 800 frames/s. Slow playback of these videos shows extremely detailed flow structures in the regimes identified. In general, the flow starts with cold liquid hydrogen flowing into a warm tube. Heat flows from the warm tube wall to the cold fluid; at early times, when the wall is quite warm, there is a location in the line past which the flow is all-vapor. This location depends on the residual heat stored in the tube walls and consequently on the local wall temperature. In the final steady state the system is isothermal, i.e., the fluid and wall have the same temperature, essentially equal to the boiling temperature of liquid hydrogen at the prevailing pressure in the tube. In the final state, the fluid consists of liquid and vapor, with a liquid mass fraction near 1, flowing in the bubbly regime. However, because of the liquid-vapor density contrast, the volume fraction of liquid is not near 1 which makes the image of the final state of flow display a relatively large fraction of vapor. Between the initial flow condition and the final steady state, the flow goes through a series of regimes as the tube wall cools down, with the fluid temperature decreasing with time, although not monotonically as will be seen below.

It is helpful to refer to fig. 3 and figs. 6-11 (better resolution) as visual aids. Looking through the sight glass,

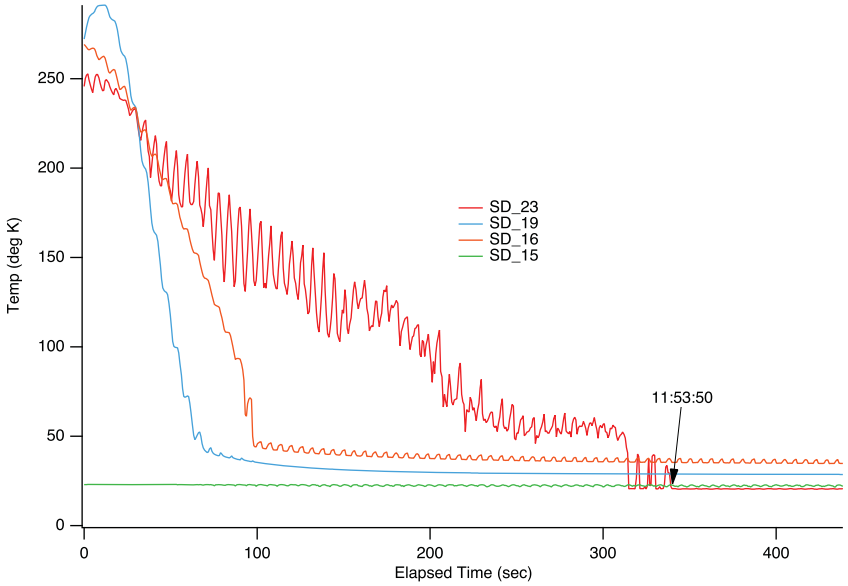

Figure 4. Time history of a medium flow '3-3' (3 seconds on, 3 seconds off) pulse test. The tag shows the time at which the stream temperature just past the sight glass, SD23, bottoms out.

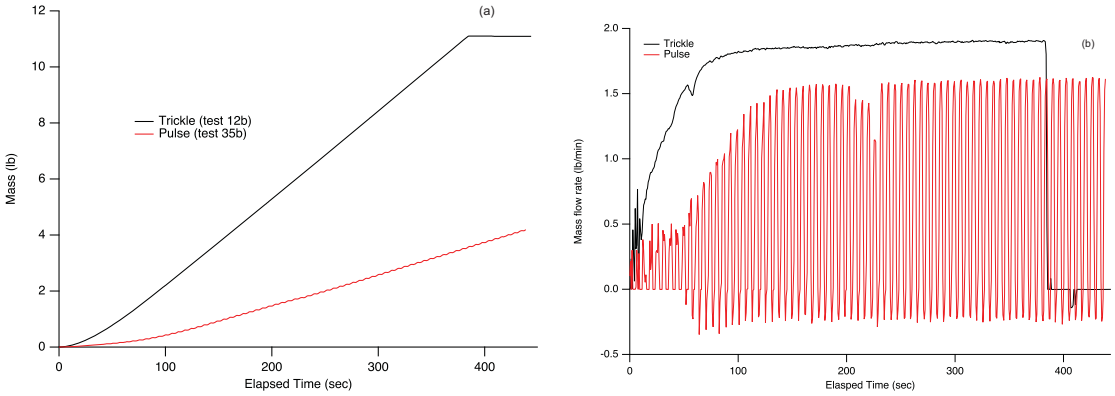

Figure 5. Time history of mass (a) and mass flow rates (b) for trickle (black lines) and pulse (red lines) tests.

the flow first appears as all-vapor. The sight glass is located far enough downstream that, at those early times, all the liquid has boiled by the time the flow reaches the sight glass. A short time later, the first drops of liquid can be seen flowing as dispersed liquid in a stream of continuous vapor. The liquid volume fraction continues to increase with time, still in the form of dispersed drops. As the liquid fraction grows, the flow regime changes from droplet-dispersed to something complex but close to slug flow. At the same time, a liquid layer begins to cover parts of the wall. This flow is almost annular, with a clear liquid layer on a significant fraction of the wall and a central vapor core. The fraction of wall covered with liquid layer increases with time. As the wall temperature drops further, the liquid fraction increases and the annular pattern is replaced by a bubbly flow, with a liquid-continuous phase and a dispersed vapor phase in the form of bubbles.

Observing the temperature evolution of the flow in time (see fig. 3), one can see a downward trend interrupted by small, short-lived upward spikes. There is a lot of structure, with spikes of many scales. In this discussion we do not address the finer-scale oscillations. Instead, we focus on the decreasing trend of the fluid temperature that occurs over periods of ~ 50 sec, which are interrupted by short upswings in temperature of about 10 to 20 deg K, lasting about 10 seconds.

The downward periods are the result of the change in heat content of the fluid replacing warm fluid at a rate faster than the rate heat can flow from the wall to the fluid stream. This happens even as the heat transfer coefficient continually increases due to the liquid fraction getting larger (the term 'heat transfer coefficient' is used loosely here, noting that there are long periods during which the wall is locally covered by vapor or liquid intermittently in a chaotic and random fashion). During the upward spikes, the cold fluid flowing into the test section is not able to remove heat

faster than the heat transfer from the warm wall into the flow. Consequently, the stream temperature rises momentarily. This could be caused by momentary and very rapid increases in the heat transfer coefficient. During all this time (and in particular, during the up-swings in fluid stream temperature) the wall temperature decreases continuously. When the wall temperature gets cold enough, the rate of heat transfer from the wall to the fluid again becomes smaller than the rate of cooling that the fluid stream can sustain; at that point, the upswing ends and the fluid temperature returns to the normal decreasing trend. In the Appendix we propose a simple model that captures the essential physics of the chill-down process.

A. Correlation between stream temperature time history and video of medium flow trickle flow test

A comparison of the time history of the stream temperature after the sight glass (SD23) in trickle flow (fig. 3) and the video of that test shows some interesting correlations that we discuss in this section. A similar comparison in a pulse test may in principle be made, but the pulsing fluctuations would obscure small but physically important features of the temperature time history.

All references correspond to the number tags in fig. 3. The video shows that the test starts with all vapor flowing by the sight glass (fig. 6). This is because, at early times, the cold liquid has evaporated completely by the time it reaches the sight glass location. During this stage, stream temperature SD23 drops monotonically until point 1. Between points 1 and 2, droplets of liquid hydrogen begin to appear in the field of view, their number density increasing with time (fig. 7). The number density of liquid drops continues to increase between 2 and 3. Between 3 and 4 there is a break in the rate of decrease of SD23. First, SD23 adopts a plateau shape, followed by a drop-off that ends at 4. The video shows the onset of liquid on the wall, though this behavior is clearly intermittent (fig. 8). From 4 to 5 the flow transitions from droplet-dispersed to annular. We can detect the transition by the presence of liquid on the wall; the fraction of tube wall covered with liquid increases with time. All this time the flow is quite chaotic and it is hard to visualize flow structure when playing the video at the original 800 fps speed. Flow structure may be gleaned by slowing down or even stopping the video. The annular flow evolves continually after 5 (fig. 9). Dark flow packets alternate with lighter regions of flow through the sight glass between 6 and 7, with the frequency of clear packets increasing around 7 (fig. 10). The flow after this point shows a slightly thicker liquid layer at the wall all the time. The end flow state is mostly annular after bottoming out at 8, see fig. 11. This end flow structure persists permanently without changes to test conditions. In a few tests the pressure downstream was raised by closing a valve downstream of the area included in the schematic of fig. 1 which caused the saturation temperature to increase and the vapor in the "cold" stream to condense. After raising the downstream pressure, the liquid fraction approached 1.

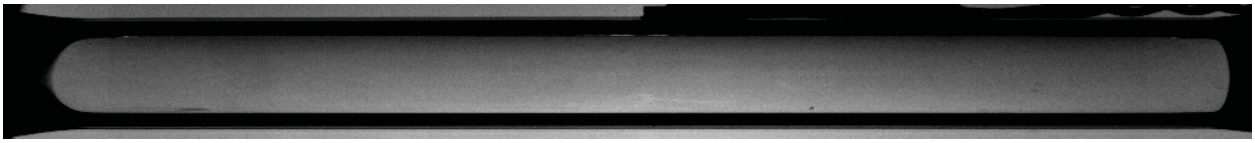

Figure 6. Frame from medium trickle flow test, showing all-vapor flow early on, between time zero and point 1 in fig. 3. Flow direction is left to right.

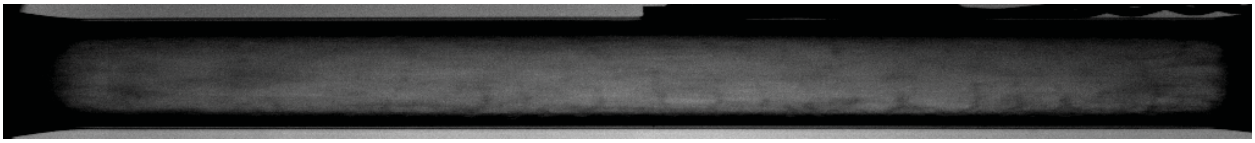

Figure 7. Frame from medium trickle flow test, showing the appearance of the first liquid droplets, between points 1 and 2 in fig. 3. Flow direction is left to right.

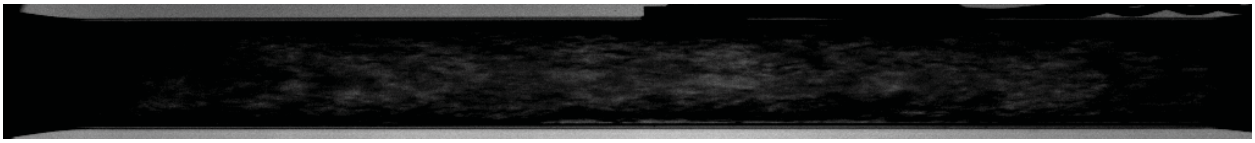

Figure 8. Frame from medium trickle flow test: a section of lower wall in the image is covered with liquid during a short instant. The liquid appears as clear thin layers next to the wall, between points 2 and 3 in fig. 3. Flow direction is left to right.

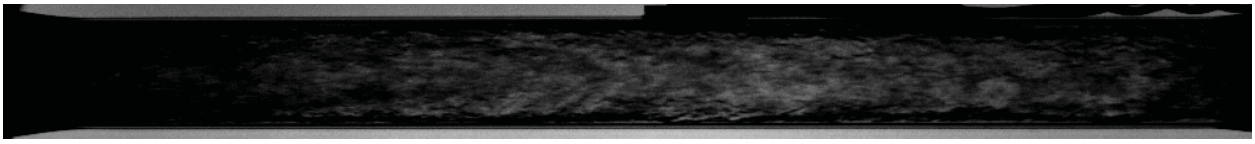

Figure 9. Frame from medium trickle flow test: flow is well on its way to annular flow, just after point 5 in fig. 3. Flow direction is left to right.

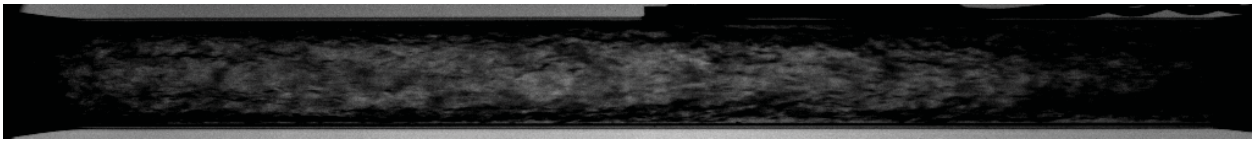

Figure 10. Frame from medium trickle flow test: a clear packet occupies most of the image, around point 7 in fig. 3. A dark packet is about to exit the field of view on the right. Annular flow has thicker liquid at the wall. While lighting is not uniform and makes the image center brighter, the dark-light packet in this image can be determined by looking at the evolution in the video recording. Flow direction is left to right.

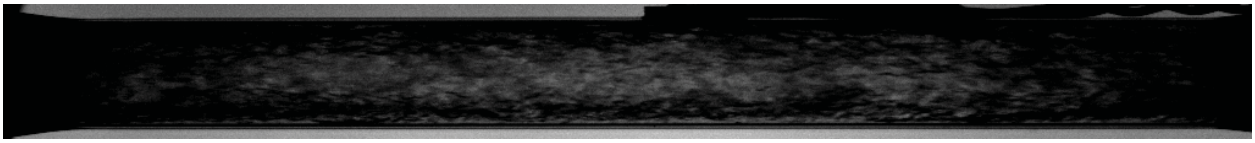

Figure 11. Frame from medium trickle flow test: End state of flow after bottom out, after point 8 in fig. 3. Annular flow is well established with relatively low vapor mass fraction. Compare the extent of the liquid layer on the wall and the structure in the core with the same features in fig. 10. Flow direction is left to right.

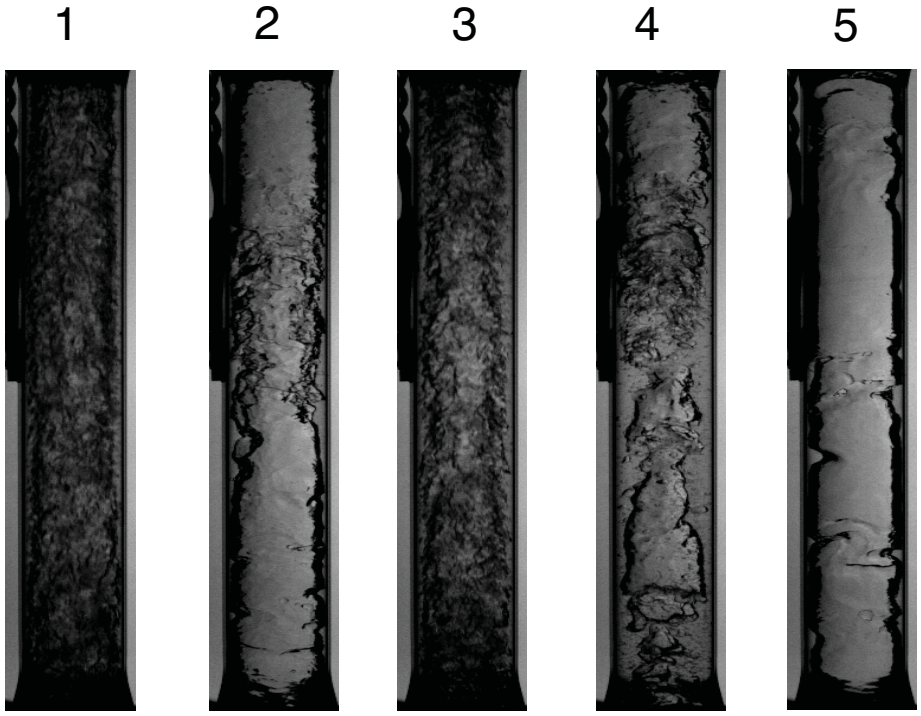

Figure 12. Series of frames from a medium flow, 3-3 pulse chilldown test. The numbering reflects chronological order, but all pictures are taken just before or just after the time at bottom out. The diameter/length ratio has been increased for clarity. 1: Annular flow before, but close to, final steady state; 2: Vapor receding upstream before, but close to, final steady state; 3: Annular flow after, but close to, final steady state; 4: Vapor receding upstream after, but close to, final steady state; 5: Another instance of vapor receding upstream after, but close to, final steady state. Flow direction is up.

B. Pulse flow chill-down

The video from a 3-3 pulse test (i.e., 3 seconds on and 3 seconds off) conveys information about the time-evolution of the system state after each flow stop in a pulse. Here we examine the flow before and after bottoming out at the final steady state. Fig. 4 shows the time history of SD23, the stream temperature measured just downstream of the sight glass. The structure of the temperature history is consistent with that seen in trickle flow tests (fig. 3), but with superimposed fluctuations from the flow pulsing. Fig. 12-1 shows the annular flow structure typical of the flow before but very close to final steady state. When the flow stops between pulses, the vapor retreats upstream (top to bottom in the images). Fig. 12-2 shows a typical image of the flow after stopping between pulses, but before the temperature SD23 has reached the final steady state. We now examine the flow and stopped images after SD23 has reached the final steady state and compare them with the corresponding images before steady state. Figs. 12-3 and 12-4 show annular flow and vapor receding, respectively, after SD23 has reached the final steady state. Both the annular flow and the stopped flow exhibit more liquid fraction than the annular flow before steady state. Fig. 12-5 shows another view of the stopped flow after bottom out, taken in the same period of stopped flow shown in fig. 12-4 but slightly later than that image.

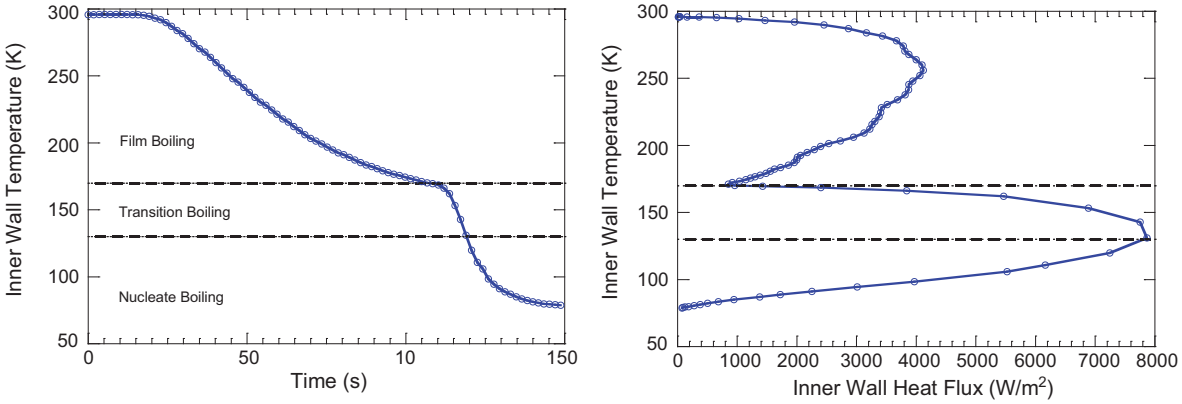

Figure 13. Time history of the inner wall temperature (left) and heat flux curve (right), for a 'low' Re ($= 3.5 \times 10^3$) trickle test of Hu *et al.*[10]. The time history exhibits an elbow at the boundary between film and transition boiling. The heat flux scale amounts to 42.3 Btu/min.ft^2.

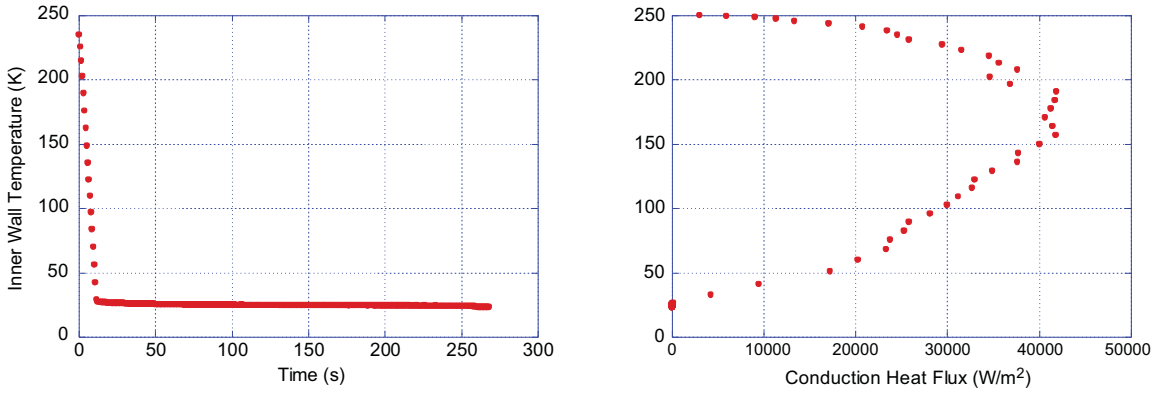

Figure 14. Time history of the inner wall temperature (left) and heat flux curve (right), for a medium flow ($G \approx 2$ lbs/min) 'high' Reynolds number ($Re = 1.04 \times 10^5$) trickle test from this work. Both these plots conform to the portion of fig. 13 seen in the transition and nucleate boiling phases. The heat flux scale amounts to 264.3 Btu/min.ft^2.

V. Comparison with low Reynolds number chilldown

Typical Re for trickle tests performed in Prof. Chung's lab at the University of Florida are $\lesssim 4000$.[6,10] By contrast, our trickle tests run at typical values of $Re \sim O(10^5)$. Figs. 13-14 show typical inner wall temperature histories and heat flux vs. inner wall temperature plots in Hu's *et al.*[10] and our trickle tests, respectively. The outer wall temperature

was measured as a function of time, and the theory of Burggraf[15] was used to calculate the inner wall temperature, assuming that the outer wall is insulated. A heat flux, representing a rate of heat content loss (or gain) from the wall into the fluid (or viceversa), can be evaluated at the inner wall in terms of the time derivatives at the outer wall, $\partial^n T/\partial t^n (r = r_o)$ for $n \geq 1$. In our tests, the outer wall sustained parasitic heat leaks from the warmer surroundings into the tube, mainly by radiation. The radiation heat flux is estimated using standard radiation view factors, the surrounding chamber temperature and the outer wall temperature $T_o(t)$. The heat flux at the inner wall transferred to (from) the fluid is the sum of the heat content loss (gain) rate of the solid wall and the heat leaks.

Figs. 13-14 show the low and high Re cases. Besides the obvious larger maximum heat flux at higher Re, which results in higher heat transfer coefficients, the high Re tests are notable because they do not exhibit a region of film boiling that is well defined in the low Re tests. This is particularly evident in the plots of wall temperature vs. heat flux, where our tests only show the phase that corresponds to transition and nucleate boiling.

VI. Summary and conclusions

By examining video recordings together with time histories of the stream temperature next to the field of view (fig. 3), we have been able to correlate features of the plot of the stream temperature vs. time with information about the flow regime structure gleaned from the video. In particular, we were able to propose a connection between the non-monotonically decreasing stream temperature and changes in quality which drive discrete increases in heat transfer coefficient; see Appendix for a supporting calculation.

While we never obtained zero-quality flow (i.e., all-liquid), the flow approached zero-quality every time the downstream pressure was raised above the baseline by throttling a valve downstream of the diagram in fig. 1. While we cannot rule out heat transfer from parasitic heat leaks (conduction through components that breach the vacuum jacket, or radiation from the surroundings, for example) the lack of zero-quality flow after bottom out is the result of a complex set of variables, including degree of subcooling in the tank, rate of heat leak into the chill line, rate of flow, and pressure level in the line. The fact that we could approach zero-quality by raising the downstream pressure demonstrates that it is possible, in principle, to get to that point –but the baseline settings in our tests did not allow it. Other strategies different from raising downstream pressure, such as increased subcooling, may achieve the same result.

At the high Reynolds numbers of these tests ($Re \approx 10^6$), boiling of cold cooling liquid is dominated by transition and nucleate boiling, at least at the location downstream from the sight glass where the stream temperature is measured. This is quite different from the regime of Chung and collaborators where the flow Reynolds numbers are considerably lower $Re \lesssim 4 \times 10^3$, and transition and film boiling play an important role.[10] However, since our tests are not exhaustive, the possibility that film boiling might be present at some other location cannot be ruled out.

Appendix

Using a simple model, we present a plausible cause for the humps observed in the time history of the fluid temperature. If a cold fluid is injected into a warm pipe filled initially with warm fluid, the wall and the fluid temperature at a fixed location must both decrease in time, at least after all the warm fluid initially in the tube has been expelled. Our conjecture was that, as the liquid fraction increases, so does the effective heat transfer coefficient, which in turn would cause the fluid temperature to increase briefly (due to improved heat transfer from the warm wall), and then continue its downward trend until the steady state is reached at the temperature of the incoming cold fluid. This argument only relies on the increase in heat transfer coefficient, hence it does not require phase change as a cause for the increase.

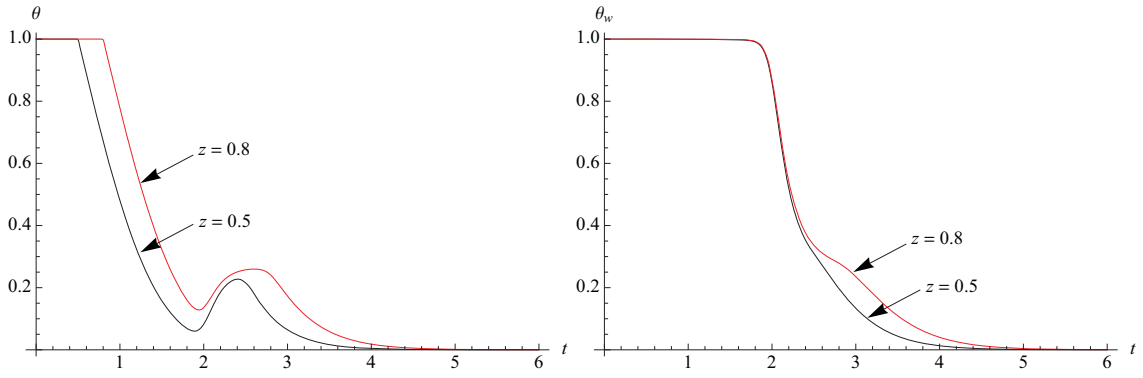

Figure 15. Fluid (a) and wall (b) temperatures at two axial z-locations, as a function of time. Clearly defined humps mark short-lived fluid temperature increases in response to a 1000-fold increase in heat transfer coefficients at $t = 2$.

In our simple model the fluid moves as plug flow with uniform velocity U. We neglect heat conduction in the fluid because it is well mixed by turbulence. Since the solid wall thickness is much smaller than its length, we assume constant temperature across the thickness (i.e., we neglect radial conduction) and retain axial conduction. With these assumptions, the cross-section averaged dimensionless problem for the fluid temperature θ and wall temperature θ_w is:

$$\frac{\partial\theta}{\partial t} + \frac{\partial\theta}{\partial z} = H(\theta_w - \theta) \tag{1a}$$

$$\frac{\partial\theta_w}{\partial t} = \frac{1}{Pe}\frac{\partial^2\theta_w}{\partial z^2} + H_w(\theta - \theta_w) \tag{1b}$$

$$\theta(z,0) = 1, \;\; \theta(0,t) = 0, \;\; \theta_w(z,0) = 1, \;\; \theta_{w_z}(0,t) = \theta_{w_z}(1,t) = 0 \tag{1c}$$

where temperatures have been made non-dimensional with the initial warm fluid-wall temperature, T_i, and the axial distance, z, with the tube length L; subscript z denotes differentiation; $H \equiv 2hL/R\rho c_p U$, $H_w \equiv hL/\delta\rho_w c_{p_w} U$ and $Pe \equiv \alpha/LU$ is the Péclet Number –a ratio of conductive to convective heat transfer. Here, h is the conventional fluid-wall heat transfer coefficient; L, R denote the tube length and radius; $\rho, \rho_w, c_p, c_{p_w}$ are the fluid and wall densities and heat capacities; δ is the wall thickness, assumed to be $\ll R$; and α is the heat diffusivity of the wall.

In order to simulate the change in h, we define time-dependent quantities H, H_w as

$$H = \frac{H_1 + H_2}{2} + \frac{H_2 - H_1}{2}\tanh\frac{t - t_0}{\delta}, \tag{2a}$$

$$H_w = \frac{H_{w_1} + H_{w_2}}{2} + \frac{H_{w_2} - H_{w_1}}{2}\tanh\frac{t - t_0}{\delta}. \tag{2b}$$

This form introduces a very rapid change over an interval $O(\delta)$ around $t = t_0$ between values with subscript 1 (at $t \ll t_0$) and those with subscript 2 (at $t \gg t_0$).

Using realistic property values, and the Dittus-Boelter correlation for Nusselt number in interior turbulent pipe flow, we use the following values for our example:

$$t_0 = 2, \;\; \delta = 0.1, \;\; H_1 = 1.4 \times 10^{-3}, \;\; H_2 = 1.4, \;\; H_{w_1} = 4 \times 10^{-3}, \;\; H_{w_2} = 4, \;\; Pe = 80. \tag{3}$$

(Note that the ratio H/H_w =constant if only h is to change value.)

Fig. 15 shows the effect on the fluid temperature at two axial locations, when the heat transfer coefficient increases by a factor of 1000 at $t = 2$. Initially, the fluid in the tube and the wall are warm, at $\theta = \theta_w = 1$. The fresh, cold fluid enters at $z = 0$ with temperature $\theta = 0$. The long-time steady state is isothermal with $\theta = \theta_w = 0$. The time when fluid temperature starts to drop at a given z location is given by $t = z$, i.e. the time when fresh fluid reaches the z-location. Even though the wall temperature seems constant for $t < 2$ (see fig. 15-b), it does drop very slowly due to the small value of h during the period of time $z < t < 2$. During the fluid temperature hump, the wall temperature drop rate is slower.

References

[1]Sloop, J. L., "Liquid Hydrogen as A Propulsion Fuel 1945-1959," Tech. rep., NASA Technical Memorandum SP-4404, Washington, DC, 1978.

[2]Schuster, J. R., Howell, D. J., Lucas Jr, S. L., Haberbusch, M. S., Gaby, J. D., Van Dresar, N. T., and Wadel, M. F., "Cold flow testing of revised engine chilldown methods for the Atlas Centaur," *Proceedings of the 32nd Joint Propulsion Conference and Exhibit*, AIAA Paper 96-3014, Lake Buena Vista, FL, 1996.

[3]Santiago, J. R., "Evolution of the RL10 Liquid Rocket Engine for a New Upperstage Application," *Proceedings of the 32nd Joint Propulsion Conference and Exhibit*, AIAA Paper 96-3013, Lake Buena Vista, FL, 1996.

[4]Van Lerberghe, W. M., Emdee, J. L., , and Foust, R. R., "Enhanced Reliability Features of the RL10E-1 Engine," *Proceedings of the 48th International Astronautical Congress*, IAF Paper 97-S203, Turin, Italy, 1997.

[5]Silke, K. and Jackson, T., "Frequently Asked Questions About Rocket Engine Reliability Programs," *Proceedings of the Annual Reliability and Maintainability Symposium*, Jan. 18-Jan. 21 1999, Washington, DC, 1999.

[6]Yuan, K., Ji, Y., Chung, J., and Shyy, W., "Cryogenic Boiling and Two-Phase Flow during Pipe Chilldown in Earth and Reduced Gravity," *Journal of Low Temperature Physics*, Vol. 150, No. 1-2, 2008, pp. 101–122.

[7]Kawanami, O., Nishida, T., Honda, I., Kawashima, Y., and Ohta, H., "Flow and heat transfer on cryogenic flow boiling during tube quenching under upward and downward flow," *Microgravity Science and Technology*, Vol. 19, No. 3-4, 2007, pp. 137–138.

[8]Kawanami, O., Azuma, H., and Ohta, H., "An experimental study on flow patterns and heat transfer characteristics during cryogenic chilldown in a vertical pipe," *International Journal of Heat and Mass Transfer*, Vol. 50, 2007, pp. 3490–3497.

[9]Zhang, P. and Fu, X., "Two-phase flow characteristics of liquid nitrogen in vertically upward 0.5 and 1.0 mm micro-tubes: Visualization studies," *Cryogenics*, Vol. 49, 2009, pp. 565–575.

[10]Hu, H., Chung, J. N., and Amber, S. H., "An experimental study on flow patterns and heat transfer characteristics during cryogenic chilldown in a vertical pipe," *Cryogenics*, Vol. 52, No. 4, 2012, pp. 268–277.

[11]Shaeffer, R., Hu, H., and Chung, J., "An experimental study on liquid nitrogen pipe chilldown and heat transfer with pulse flows," *International Journal of Heat and Mass Transfer*, Vol. 67, No. 0, 2013, pp. 955 – 966.

[12]Yuan, K., *Cryogenic Boiling and Two-Phase Chilldown Process Under Terrestrial and Microgravity Conditions*, Ph.D. thesis, University of Florida, 2006.

[13]Brennan, J. A., Brentari, E. G., Smith, R. V., and Steward, W. G., "Cooldown of Cryogenic Transfer LinesAn Experimental Report," Tech. rep., National Bureau of Standards Report 9264, Washington, DC, November 1966.

[14]Hartwig, J. W., Chato, D. J., McQuillen, J. B., Vera, J., Kudlac, M. T., and Quinn, F. D., "Liquid Acquisition Device Outflow Tests in Liquid Hydrogen," *25th Space Cryogenics Workshop*, June 23-June 25 2013, Girdwood, AK, 2013.

[15]Burggraf, O. R., "An exact solution of inverse problem in heat condition theory and application," *J. Heat Transfer*, Vol. 86, 1964, pp. 373–382.